

Dust formation and evolution in a Ca–Fe–SiO–H₂–O₂ vapour phase condensation experiment and astronomical implications

Frans J. M. Rietmeijer,^{1*} Aurora Pun¹ and Joseph A. Nuth III²

¹*Department of Earth and Planetary Sciences, MSC03-2040, 1-University of New Mexico, Albuquerque, NM 87131-0001, USA*

²*Astrochemistry Laboratory, Solar System Exploration Division, Code 691, NASA Goddard Space Flight Center, Greenbelt, MD 20771, USA*

Accepted 2009 February 25. Received 2009 February 19; in original form 2008 November 21

ABSTRACT

Here, we report on a kinetically controlled vapour phase condensation experiment using a low-calcium Ca–Fe–SiO–H₂–O₂ vapour. Under these conditions of extreme disequilibrium, the condensate properties become predictable. They are amorphous solids with (predictable) deep metastable eutectic compositions. This study also shows how chemical evolution of the condensate grains will lead to chemically complex amorphous solids. The highly disordered structure of the deep metastable eutectic condensates is the very key to this predictable chemical evolution to grains with a silicate mineral composition, yet being amorphous. We compare our results with astronomical observations of dust around young stellar objects.

Key words: astrochemistry – methods: laboratory – Solar system: general – planetary systems: protoplanetary discs.

1 INTRODUCTION

In our first condensation experiment, a massive clump of condensed magnesiosilica evolved into a porous aggregate of forsterite and enstatite crystallites and embedded nanometer-scale tridymite plates during post-condensation heating (Rietmeijer, Nuth & Mackinnon 1986). This aggregate resembled a chondritic porous, aggregate interplanetary dust particle (IDP). These IDPs are debris from active comets (Bradley & Brownlee 1986). The experiment did not say much about solar nebula condensation but it showed that condensates can be the precursors to IDP-like particles (Rietmeijer 1998). It was thought that circumstellar dust condensates would be small grains of simple metal-oxides (e.g. SiO₂, MgO) formed under disequilibrium conditions (Donn 1979) that were arranged on stands or ‘necklaces’ in open, three-dimensional networks (Stephens & Kothari 1978; Duley, Millar & Williams 1979).

Subsequent condensation experiments on a wide range of vapour compositions in the improved condensation flow apparatus (CFA) (Nelson et al. 1989; Nuth, Rietmeijer & Hill 2002) produced nanometer-scale condensate grains that (i) are amorphous simple metal-oxides and (ii) arranged in open, three-dimensional networks of intertwined ‘necklaces’ (Rietmeijer, Nuth & Karner 1999a; Rietmeijer et al. 2002). The experiments show that vapour phase condensation is defined by metastable equilibrium.

The MgO–SiO₂ system also includes the minerals enstatite (MgSiO₃) and forsterite (Mg₂SiO₄) that exist in comets and nebulae around Young Stellar Objects and comets (Bouwman et al. 2001; Molster & Waters 2003; Wooden, Harker & Brearley 2005). These

minerals typically do not form in the condensation experiments but rare well-ordered forsterite (Mg₂SiO₄) nanograins were found in some condensed magnesiosilica samples (Molster & Bradley 2001; Rietmeijer, Nuth & Nelson 2004) probably by oxidation of condensed deep metastable eutectic (DME) Mg₂Si alloy grains that were found in another magnesiosilica smoke (Kimura, private communication).

During the short time of a condensation experiment, there are complex oxidation–reduction reactions and condensed grains with end-member compositions of equilibrium phase diagrams collide, fuse and form amorphous chemically complex nanometer-scale grains larger than the original simple metal-oxide condensates. These ‘chemically complex’ grains had clear preferences for two or more specific compositions of ferrosilica (Rietmeijer & Nuth 1991), aluminosilica (Rietmeijer & Karner 1999), magnesiosilica (Rietmeijer et al. 2002), calciosilica (Rietmeijer et al. 2008a) and ferroalumina (Rietmeijer, Pun & Nuth 2008b) condensates.

The preferred compositions of these condensates are systematically between the compositions of two adjacent stable eutectics in the appropriate equilibrium phase diagram (Fig. 1). For example, the condensate compositions in an Al–SiO–H₂–O₂ vapour are defined in the Al₂O₃–SiO₂ phase diagram (Rietmeijer & Karner 1999).

The DME compositions of the amorphous condensates match, among others, a serpentine dehydroxylate, e.g. Fe₃Si₂O₇, or a smectite dehydroxylate composition. Their metal-oxide to SiO₂ ratio resembles those of the layer silicate minerals but with the (OH)[−] groups of layer silicates substituted by oxygen (Nuth, Hallenbeck & Rietmeijer 2000a; Nuth et al. 2000b, 2002; Rietmeijer et al. 2006, 2008a,b).

Experiments with two metal-oxide vapours yield amorphous condensate grains that are

*E-mail: fransjmr@unm.edu

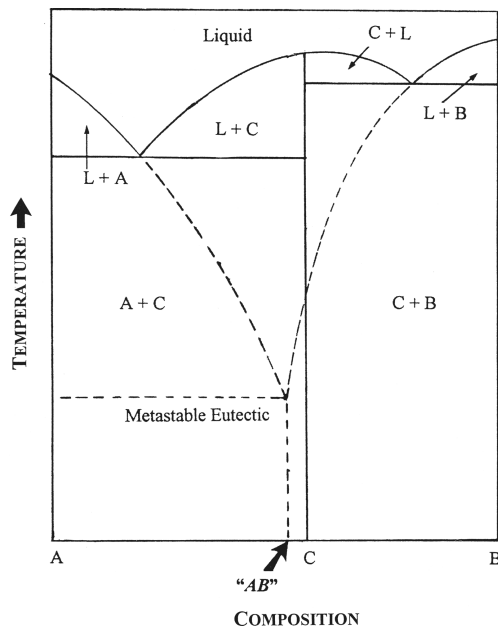


Figure 1. Hypothetical binary equilibrium phase diagram for two compositions *A* and *B* showing the position of the (deep) metastable eutectic point with the “*AB*” composition at the intersection of the metastable extensions of the liquidus surface (dashed lines) in between the compositions of both (stable) eutectic points on the liquidus surface at the top of the diagram (solid lines). Modified after Rietmeijer & Nuth (2000).

(i) Pure oxides: silica (SiO_2), MgO , FeO , Fe_2O_3 and alumina (Al_2O_3 ; Volten et al. 2007).

(ii) Binary oxide grains with DME compositions, ferroalumina grains (Rietmeijer et al. 2008b) and chemically evolved grains with a stoichiometric mineral composition, *viz.* wollastonite, CaSiO_3 , a pyroxene mineral (Rietmeijer et al. 2008a) and Fe-cordierite (Rietmeijer et al. 2006).

Condensation experiments with three metal-oxide vapours have an additional degree of freedom that is a first step towards the formation of amorphous compounds with evolved chemical compositions, and to the formation of minerals in nebulae around Young Stellar Objects (Nuth et al. 2000b; Bouwman et al. 2001; Nuth et al. 2002; Molster & Waters 2003) and dust aggregates ejected from active comets (Hadamcik et al. 2007; Volten et al. 2007).

Condensation in $\text{Mg-Fe-SiO-H}_2\text{-O}_2$ vapours produced DME magnesiosilica and ferrosilica grains but no mixed ferromagnesiosilica grains (Rietmeijer et al. 1999a). Yet, common constituents in cometary dust have unique ferro-magnesiosilica compositions due to agglomeration, mixing and fusing of magnesiosilica and ferrosilica condensates (Rietmeijer 2002). We hypothesized that mixing occurred along lines connecting solids with DME compositions. Testing the hypothesis in condensing $\text{Al-Fe-SiO-H}_2\text{-O}_2$ vapours produced amorphous aluminoferrosilica grains that behaved in a manner consistent with our hypothesis but the overwhelming abundance of condensate was hiding the details of the process (Rietmeijer et al. 2006). The study highlighted that cooling rates during the period of heat dissipation following the onset of vapour phase condensation will affect the structural and chemical evolution of condensed grains in these experiments.

In this paper, we trace the onset of chemical evolution by mixing condensates with DME compositions during condensation of a low-CaO $\text{Ca-Fe-SiO-H}_2\text{-O}_2$ vapour wherein we anticipated subtle thermal effects during heat dissipation. We report on condensate

grains with a CaFeO DME in the pseudo-binary CaO-FeO system. The condensates will contain both ferrous (FeO) and ferric (Fe_2O_3) iron due to variable oxidation conditions in the vapour condensation experiment (Rietmeijer, Nuth & Karner 1999b; Rietmeijer et al. 2006). The ‘ FeO ’ designation is used to indicate the presence of both iron oxides. Understanding chemical evolution of vapour phase condensates will advance our knowledge on the formation of amorphous metastable solids with predictable compositions in condensing circumstellar nebulae, including the solar nebula.

2 METHODS

2.1 Vapour phase condensation

Laboratory condensation of $\text{Ca-Fe-SiO-H}_2\text{-O}_2$ vapour was conducted in the CFA at the NASA Goddard Space Flight Center. The smoke particles condensed from a gas rapidly cooling to approximately room temperature after passing through a hydrogen oxygen flame. The gas composition is typically more than 80 per cent hydrogen with variable amounts of silane, iron pentacarbonyl (in helium) and trimethyl aluminium (in helium) to obtain the desired metal-oxide bulk composition. The gases are mixed thoroughly by passing through a chamber filled with glass beads prior to injection into the furnace. The furnace is a resistively heated alumina tube maintained at a constant temperature (~ 800 K) where the reactive gas stream is mixed with oxygen at controlled flow rates to produce a hydrogen flame from which dust condenses after emerging from the furnace. The oxygen fugacity is not buffered during condensation. The gas passes through a hydrogen-oxygen flame front (~ 1500 K) within the 1-inch diameter heated furnace (~ 800 K) then exits to a large (4-inch) room temperature collection region. At the gas flow rates used in typical experiments, this transition might require as long as from 5 to 10 ms, though the grains could cool more slowly due to inefficient heat transfer to their surroundings. The condensed smoke was collected on an aluminium substrate, then carefully removed from the CFA, and placed in clean vials for shipment and analysis.

2.2 Transmission electron microscope analysis

A small amount was removed from the vials and placed in a clean mortar. Gentle pressure was applied to loosen the deposit. The powder was embedded in epoxy (Spurrs) following standard procedures in the Electron Microbeam Analysis Facility (UNM). Serial ultra thin (70 nm) sections were cut from epoxy stubs with embedded smoke material. The sections were placed on a thin holey carbon film supported by 200 mesh standard TEM Cu grids for analyses using a JEOL 2010FM high-resolution transmission electron microscope (HRTEM) that operated at 200 keV accelerating voltage and was equipped with a LINK ISIS energy dispersive spectrometer (EDS) with an ultra thin-window for quantitative chemical analyses, including oxygen, using the Cliff–Lorimer thin film procedure. The analytical probe was 5 or 10 nm but smaller than the individual grains. The reported oxide values are within the 2σ range. A slow-scan CCD capable of on-line, low-dose TEM imaging was used to record the location of each grain. The images were used to cull ‘questionable’ data, e.g. due to overlapping grains that initially went unnoted using a through-focus technique to detect condensed grains smaller than the section thickness. Grain-sized diameters with a relative error of ~ 10 per cent were measured from computer-stored images; the amorphous or crystalline nature was established by selected area electron diffraction. The statistical data are accepted at 95 per cent confidence limit. All iron was calculated as FeO

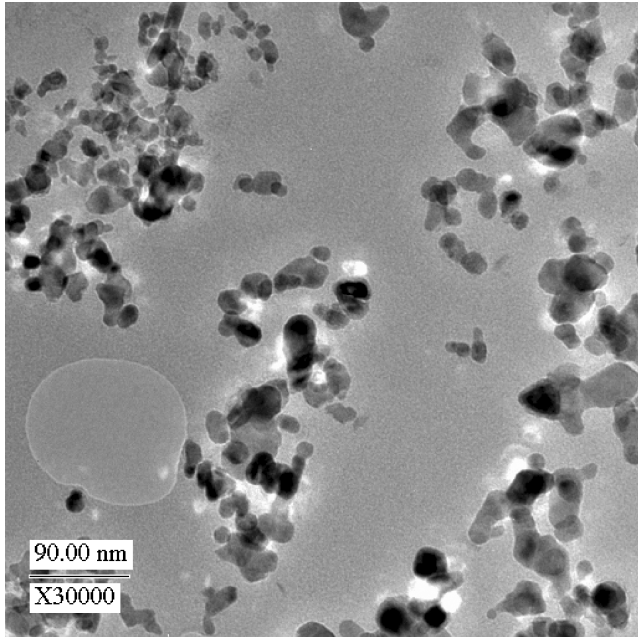


Figure 2. Transmission electron microscope image showing a planar cut through the open, or porous, three-dimensional networks of the condensed sample and individual grains (black/dark grey) arranged on short strands. The grey background is epoxy applied for sample preparation. For HRTEM analysis, the ultra thin sections are placed on a holey carbon film. The circular structure is a hole in the support film. White spots indicate sample loss. The scale bar is 90 nm.

although the compositions are constrained in the pseudo-ternary system $\text{CaO-FeO/Fe}_2\text{O}_3\text{-SiO}_2$.

3 OBSERVATIONS

Condensation of this $\text{Al-Fe-SiO-H}_2\text{-O}_2$ vapour produced a very open (porous) structure of clusters wherein the individual grains are arranged on short chains (Fig. 2). The smooth grain outlines and variable sizes are readjustments to lowering the surface free energy.

3.1 Binary metal-oxides

3.1.1 Calciowüstite

These amorphous, somewhat elongated, CaFeO grains range from 30 to 60 nm (Table 1). Vestiges of small condensate grains are preserved in some grains. The compositions match calciowüstite, an orthosilicate-iron oxide (Fig. 3).

3.1.2 Calciosilica grains

The compositions of these amorphous, irregularly shaped and (sub) spherical condensates define three Gaussian distributions at 88.1, 25.5 and 7.9 CaO wt per cent (Fig. 3; Table 1); two populations are represented by only three grains.

3.1.3 Ferrosilica grains

The compositions of these abundant amorphous and poorly ordered grains define several Gaussian distributions for populations $N > 2$. Small errors in assigning population ranges carried forward and caused a residual group for 6 per cent of the data $5 < \text{FeO} < 90$ wt per cent (Table 2). This artefact of data reduction has little effect on the population means (Table 2). The grains that range from 4 to 50 nm in these populations have lognormal size distributions (Table 2). The population, $\text{FeO} = 93.2$ wt per cent, has a Gaussian size distribution.

4 TERNARY METAL-OXIDES

4.1 Low-CaO ($1.5 \leq \text{CaO} \leq 5$) CaFeSiO grains

These amorphous and poorly ordered amorphous grains define two groups of low-CaO CaFeSiO compositions (Fig. 3). The first group ($\text{CaO} < 3$ wt per cent) includes four distinct populations; the second has two populations defined by FeO content (Table 3). The grain sizes form Gaussian distributions, except the population $\text{FeO} = 72.8$ wt per cent that is slightly skewed (Table 3).

4.2 High-CaO (5–20 wt per cent) CaFeSiO grains

They are amorphous and form two poorly defined populations that mainly differ in the FeO content (Fig. 3; Table 4). A Student's *t*-test finds that the hypothesis cannot be rejected that these grains are not from grain-sized populations with different mean values.

4.3 Low-silica (~ 3 -wt per cent SiO_2) CaFeSiO grains

A dense cluster of individual, uniformly low-silica CaFeSiO condensate grains near the iron oxide corner (Fig. 3) has distinct CaO wt per cent populations (Table 5). The large populations have about equal amounts of round and elongated grains supporting grain growth in small chains and clusters. About a quarter of grains in the population $\text{CaO} = 7.2$ wt per cent contain vestiges of small condensate grains.

Table 1. CaFeO (calciowüstite) and CaSiO condensate compositions (wt per cent), grain size [nm; mean (μ) \pm standard deviation (σ)] and range and number of grains in each population (N).

FeO (wt per cent)	CaO (wt per cent)	SiO ₂ (wt per cent)	Size	Range	N
6.1 ± 0.4	3.9 ± 0.4	–	45.0 ± 12.9	30–60	5
–	88.1 ± 2.6	11.9 ± 27	22.5 ± 5.3	16–28	7
–	62.5	37.5	54	–	2
–	40.6	59.4	60	–	1
–	25.5 ± 6.6	74.5 ± 6.5	54.1 ± 16.5	38–71	10
–	7.9 ± 2.0	92.1 ± 2.1	40.9 ± 9.6	26–55	19

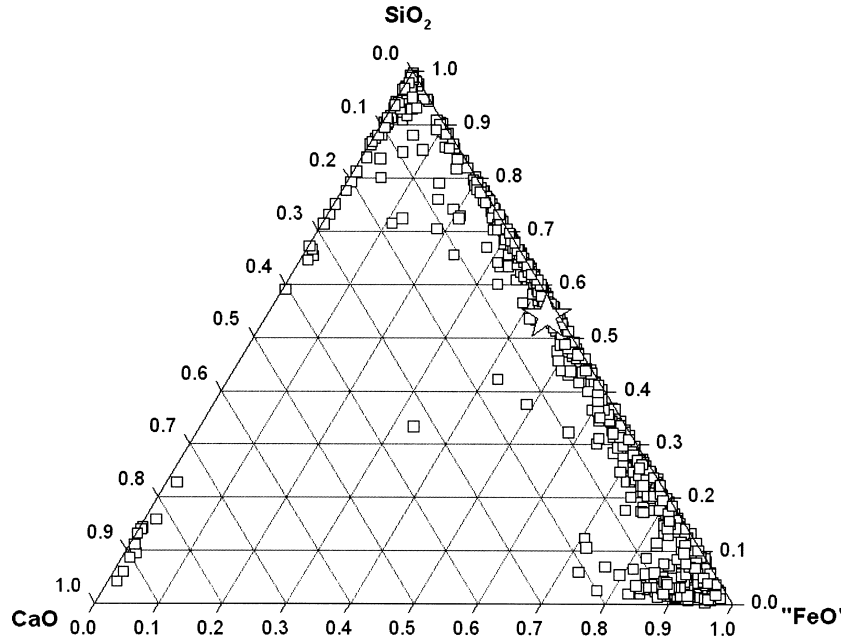


Figure 3. The individual condensate grain compositions in the samples (open squares) are presented in pseudo ternary CaO–FeO–SiO₂ diagram. The high concentrations along the ‘FeO’–SiO₂ and CaO–‘FeO’ sides of the diagram reflect the low-CaO content of the condensing Ca–Fe–SiO–H₂–O₂ vapour. Its calculated bulk composition (open star) is similar to the CI bulk composition of the Orgueil meteorite, SiO₂ = 54.2 wt per cent, FeO = 43.6 wt per cent and CaO = 2.2 wt per cent. The pure silica condensates are not indicated. These subspherical amorphous grains range from 18 to 65 nm with a mean size of 38 ± 18 nm.

Table 2. FeO wt per cent contents of ferrosilica condensate, grain size (nm) ($\mu \pm \sigma$) and range for each population (N). The population, FeO = 93.2, has a Gaussian size distribution; all other grain size populations are skewed, normal distributions indicated by modal size (nm) and skewness (S : (mean-mode)/standard deviation). ^(*): this residual population has a flat size range.

FeO (wt per cent)	Size	Range	N	Modal size; S
10.5 ± 4.2	10.3 ± 3.1	3–14	19	12.3; –0.66
31.8 ± 7.5	13.9 ± 8.4	4–50	125	8.2; 0.67
38.0 ± 4.9	15.7 ± 4.1	10–29	91	12.5; 0.80
56.2 ± 6.4	20.8 ± 8.3	11–48	43	17.1; 0.44
76.4 ± 4.6	20.9 ± 5.2	12–36	48	22.2; –0.25
$86.2 \pm 3.1^{(*)}$	26.8 ± 6.9	15–42	22	–
93.2 ± 2.4	28.6 ± 6.5	19–39	9	–

Table 3. FeO (wt per cent) contents of calcioferrosilica condensate compositions in two groups of low CaO (<5 wt per cent), the grain size (nm) ($\mu \pm \sigma$) and size range for each population (N). The modal size and S values are shown for a single slightly skewed size distribution.

FeO (wt per cent)	Size	Range	N	Modal size; S
$1.5 \leq \text{CaO wt per cent} < 3$				
12.4 ± 2.8	16.5 ± 5.1	10–21	4	NA
47.1 ± 6.6	21.2 ± 7.1	11–42	23	–
72.8 ± 6.0	20.0 ± 5.9	10–34	48	22.1; –0.35
88.7 ± 2.0	29.0 ± 7.0	24–44	8	–
$3 < \text{CaO wt per cent} \leq 5$				
38.0 ± 6.1	24.3 ± 10.0	13–41	8	–
69.1 ± 6.8	17.5 ± 6.0	9–30	19	–

Table 4. Average compositions of two high-CaO (5–20 wt per cent) calcioferrosilica condensate populations, grain size (nm) ($\mu \pm \sigma$) and size range (N).

SiO ₂	FeO	CaO	Size	Range	N
76.0	14.8	9.2	26.7 ± 10.9	14–56	13
25.3	68.4	6.3	20.9 ± 8.4	10–35	11

Table 5. The CaO (wt per cent) contents for three low-silica CaFeSiO condensate groups, grain size (nm) ($\mu \pm \sigma$) and size range for two populations (N).

SiO ₂ wt per cent	CaO wt per cent	Size	Range	N
2.6 ± 0.7	7.2 ± 1.9	28.2 ± 7.9	16–49	41
2.6 ± 0.7	12.7 ± 1.7	29.1 ± 5.1	21–41	13
2.6 ± 0.7	21	20	–	1

5 GRAIN-SIZED DISTRIBUTIONS

5.1 General

Grain-sized distributions contain information on the processes that modified some of the physical properties and how porosity affected structural evolution. The lognormal grain-sized distributions for the pure silica, calcio-wüstite, calciosilica and CaFeSiO condensates support that they grew by grain fusion, a common process to reduce surface free energy. It was facilitated in the denser grain clusters in the condensed samples. The average size, 46 ± 15 nm, of the DME CaSiO condensates (Table 1) suggests that they formed at the onset of condensation due to their refractory nature ahead of the DME ferrosilica condensates.

5.2 Ferrosilica grains

The ferrosilica condensates have skewed normal size distributions. A negative skewness (S) value indicates a population dominated by the largest grains, *viz.* The 10.5 FeO wt per cent population (Table 2) grew in isolation of newly condensing grains. Positive S -values indicate arrested grain growth. The S values (Table 2) reflect variations in porosity of the condensed sample with dense clusters and aggregates of high porosity. Additional insight into the growth process is obtained from normalized steady-state frequency versus size profiles (Baronnet 1984), *viz.* condensate grains 31.8-wt per cent FeO (Table 2) growth were a second-order process at low levels of evolving grain density. The steady-state profile for the 10.5-wt per cent FeO grains confirms diffusion controlled growth in densely packed clusters.

6 AMORPHOUS GRAIN CRYSTALLIZATION

Amorphous condensates with end-member oxide compositions often crystallize during the period of heat dissipation to tridymite (SiO_2), periclase (MgO), magh emite ($\gamma\text{-Fe}_2\text{O}_3$) and hematite ($\alpha\text{-Fe}_2\text{O}_3$) minerals. When heated after condensation, the initial adjustments of amorphous condensates will be rearrangements in the Si–O stretching and bending modes causing subtle changes in the infrared spectra (Nuth & Donn 1983, 1984; Hallenbeck, Nuth & Daukantes 1998; Hallenbeck, Nuth & Nelson 2000). With continued heating, crystallographic ordering can be traced by the appearance of low-order diffraction maxima of tridymite. In ferrosilica condensates that were not heated crystallographic ordering was independent of FeO content (Rietmeijer & Nuth 1991). This was also found for the condensed grains in this low-CaO Ca–Fe–SiO–H₂–O₂ vapour wherein it was independent of CaO and FeO contents. The grains are still poorly ordered, amorphous solids that have yet to show the high degree of crystallographic order of minerals. The chemical evolution in this condensation experiment was possible because the grains lacked crystallographic ordering.

7 DISCUSSION AND CONCLUSIONS

7.1 General

The number of DME eutectic points is determined only by the phase relationships in the equilibrium phase diagram, not by the bulk vapour composition (Rietmeijer et al. 2004, 2008a). The arithmetic mean of the condensed grain compositions in this study, $\text{SiO}_2 = 45.7$ wt per cent, $\text{FeO} = 50.0$ wt per cent and $\text{CaO} = 4.3$ wt per cent, indicates a low-CaO CaFeSiO bulk vapour composition. It explains the high amount of grains with ferrosilica DME compositions and the much fewer DME calciosilica condensates (Fig. 3).

DME condensation happens when the conditions are far from thermodynamic equilibrium when phase changes are driven by the surface properties of the condensates. The system is simply not yet large enough for the bulk material properties to take over. The predominantly round grains might argue for a liquid-like character of growing condensates with an amorphous structure. Thermal fluctuations in a cooling gas prior to the equilibrium condensation, when the grain and gas temperatures are equal, cause conditions wherein the condensation rate exceeds dust evaporation (De 1979). The condensates then have the properties of a ‘dissipate structure’ in the form of amorphous DME grains (Nuth et al. 2002) as shown in the CaO–‘FeO’– SiO_2 diagram (Fig. 4).

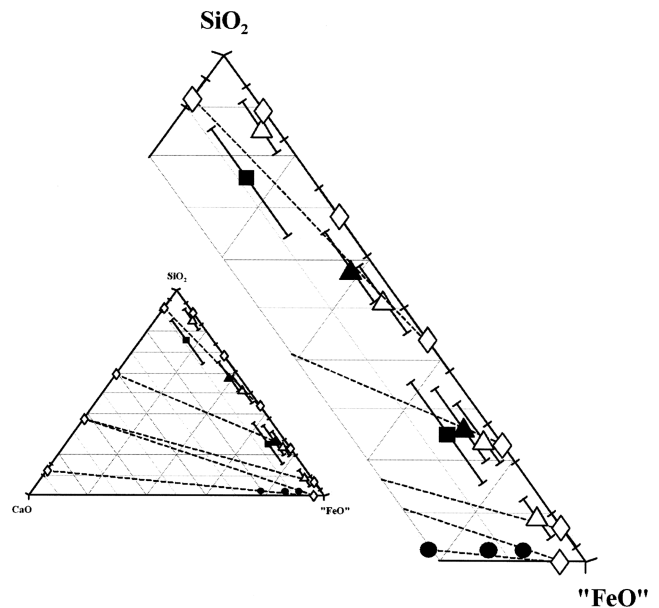


Figure 4. CaO–‘FeO’– SiO_2 ternary diagram with the locations of (i) DME FeSiO, CaSiO and CaFeO compositions (open diamonds; Tables 1 and 2) and (ii) chemically evolved CaFeSiO condensate compositions. The latter are shown as a function of CaO (wt per cent) content: (i) $1.5 \leq \text{CaO} < 3$ (open triangles), (ii) $3 < \text{CaO} \leq 5$ (solid triangles) and (iii) $5 < \text{CaO} < 20$ (solid squares) (Tables 3 and 4). Chemical evolution is along mixing lines (dashed lines) between two DME compositions across the diagram (inset: triangle). Error bars are one standard deviation; for CaFeO grains, the error bar is the size of the dots.

7.2 Deep metastable eutectic compositions

7.2.1 FeSiO and CaSiO grains

The consistency among the DME compositions from different condensation experiments (Table 6) confirms the fundamental non-equilibrium nature of these experiments including changing DME FeSiO compositions caused by variations in iron oxidation states. This change is expressed by the compositional shift from 13- to 29-wt per cent FeO for ferrosilica smectite dehydroxylate grains (Table 6) and also for ferrosilica grains with serpentine dehydroxylate compositions from $\text{FeO} = 56.2$ wt per cent (Table 6) in $\text{Fe}_3\text{Si}_2\text{O}_7$, *i.e.* the layer silicate mineral greenalite (Newman 1987) with O^{2-} replacing OH^- groups to $\text{FeO} = 76.4$ wt per cent (Table 6) for Fe^{3+} -rich cronstedtite (Newman 1987) with 81-wt per cent FeO, when all iron is recalculated to FeO. These shifting DME compositions reflect a gradual change from FeO to Fe_2O_3 as a function of decreasing vapour and condensate temperatures

7.2.2 FeCaO grains

As iron was not fully oxidized, the appropriate phase diagram is the pseudo-binary CaO–‘FeO’ phase diagram (Allen & Snow 1955) (Fig. 5; inset). It has a eutectic close to calciow ustite, $\text{CaO} \cdot 2\text{‘FeO’}$ and a calciow ustite solid solution series between 28-wt per cent CaO ($\text{CaO} \cdot 2\text{‘FeO’}$) and ~ 10 -wt per cent CaO (Eitel 1965). We replaced the original calciow ustite + liquid field of Allen & Snow (1955) by a two-liquid field and a ‘FeO’ + liquid field defined by two data points closest to the ‘FeO’ side (Fig. 5; dashed lines). The modified diagram has two stable eutectics that define (cf. Fig. 1) a DME composition between ‘FeO’ ~ 75 and

Table 6. Comparison of DME FeO and CaO condensate compositions in this study (Tables 1 and 2) and those from previous studies on FeSiO (Rietmeijer et al. 1999b; (*)Rietmeijer et al. 2006; (**)Rietmeijer et al. 1999a) and CaSiO (Rietmeijer et al. 2008a) samples, and two non-DME compositions from these sources. The non-DME ferrosilica composition (FeO = 38 wt per cent) is similar to grain composition in a ferrosilica sample heated in vacuo for 4 h at 725°C (Rietmeijer et al. 1999b). The non-DME CaO composition is uncertain. It could represent the crest of a metastable immiscibility gap in the CaO–SiO₂ system (cf. Seward 1970).

Ferrosilica DME compositions (FeO wt per cent)		Calciosilica DME compositions (CaO wt per cent)	
Previous studies	This study	Previous studies	This study
13 (7–18)	10.5	9 (1–18)	7.9
29 (15–45)	31.8		
~55(*)	56.2	42.4 (36–50)	40.6
~75(**)	76.4	72 (60–80)	62.5
87.5 (75–90)	93.2	87 (80–97)	88.1
Non-DME FeO composition		Non-DME CaO composition	
31 (25–43)	38 (10–29)		25.5

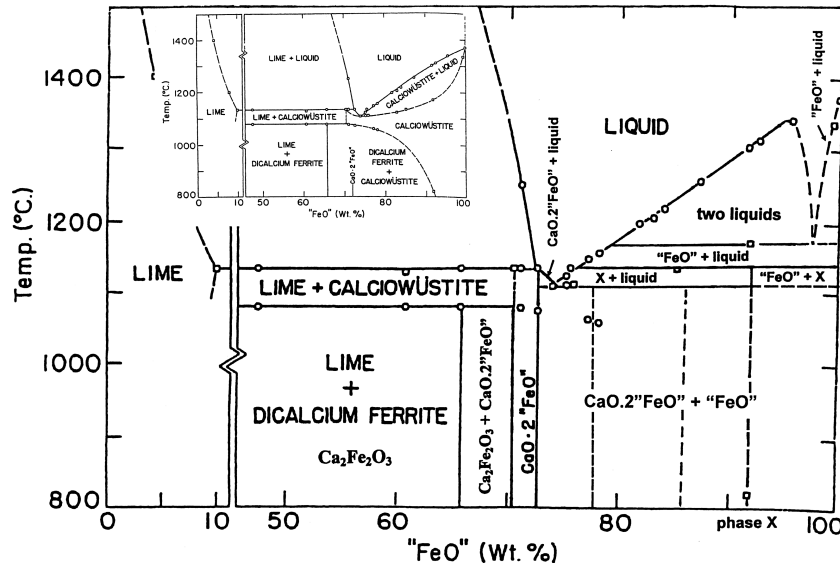


Figure 5. The modified CaO–“FeO” phase diagram where “FeO” stands for a variable FeO/Fe₂O₃ ratio based on the original experimentally determined data points (open circles and squares) from Allen & Snow (1955). The vertical dashed lines in the modified diagram delineate the metastable solid compositions in the CaO·2“FeO” + “FeO” field. The 100 per cent “FeO” phase is the mineral wüstite. The inset shows the original phase diagram. The vertical dashed lines are discrete crystalline compounds with 10- to 13.5-wt per cent CaO (Allen & Snow 1955) and 8-wt per cent CaO (CaO × 9FeO; Martin & Vogel 1934).

~99 wt per cent (Fig. 3). This DME CaFeO composition is represented by the grains with ~4-wt per cent CaO (Table 1).

7.3 Chemical evolution

Chemical evolution of the condensed grains in this low-Ca Ca–Fe–SiO–H₂–O₂ vapour is controlled by the efficiency of grain growth into larger grains of homogenized compositions among grains with (i) DME compositions in the same binary system and (ii) CaFeSiO grains along mixing lines between the DME compositions (Fig. 4). That is, (i) FeO = 56.2 wt per cent and CaO = 7.9 wt per cent and (ii) FeO = 76.4 wt per cent and CaO = 40.6 wt per cent. Slightly less dramatic along the mixing line between DME compositions at FeO = 93.2 wt per cent and CaO = 62.5 wt per cent. Finally, the low-silica CaFeSiO compositions at ~7, ~12 and ~22 CaO wt per cent (Fig. 4; Table 5) evolved along mixing lines across the ternary diagram between the CaFeO DME composition and the CaSiO DME compositions at 62.5 and 88.8 CaO wt per cent. The dashed lines (Fig. 4) show how DME ferrosilica and DME calciosilica condensates fuse along these mixing lines to produce ferrocalciosilica grains. Mixing lines may be drawn between any

pair of DME compositions in Fig. 4. Their intersections will be the loci of the most probable fully evolved amorphous grain compositions. In this sample, the grain sizes (Tables 4 and 5) indicate that chemical evolution is still in an early stage.

7.4 Astronomical implications

The CI-like bulk composition of this low-CaO Ca–Fe–SiO–H₂–O₂ vapour suggests that chemical evolution will lead mostly to low-Ca CaFeSiO grain compositions. Still, the CaFeSiO grain composition, SiO₂ = 33, FeO = 33 and CaO = 34 wt per cent, just below the centre of the diagram (Fig. 3) is identical to the olivine mineral kirschsteinite (FeCaSiO₄). This composition shows that chemical evolution and crystallisation will lead to even rare stoichiometric minerals despite the low cosmic Ca abundance. In meteorites, this olivine mineral is probably the result of parent body processing (Rubin 1997; Brearley & Jones 1998).

The results suggest that amorphous low-CaO ferrosilica grains of variable “FeO”/SiO₂ ratios might be present around young and evolved stars, including the solar nebula. Molster & Waters (2003) reported amorphous silicates (Mg/Fe ≈ 1) wherein Fe is either

dissolved in the matrix or present as inclusions in the amorphous silicate matrix. Both scenarios are supported by the results of this and previous vapour phase condensation experiments (Rietmeijer et al. 1999a,b). Amorphous silicates around young stars appear to have stoichiometric orthopyroxene compositions while around evolved stars they appear to have stoichiometric olivine compositions but the data have no information on the presence of Ca or Al (Molster & Waters 2003).

The chemical evolution of DME condensates with concomitant grain size increases is still in an early stage in our experiment. Still, the evolved grains, $3 < \text{CaO wt per cent} \leq 5$, and $\text{FeO} = 69.1$ wt per cent (Table 3), and high-CaO grains with $\text{FeO} = 68.4$ (Table 4) are stoichiometric olivine compositions. The evolved amorphous condensates, $3 < \text{CaO wt per cent} \leq 5$ and $\text{FeO} = 47.1$ wt per cent (Table 3) have a stoichiometric orthopyroxene composition. The results confirm the presence of solids that are amorphous, low-Ca olivine and pyroxene around young and evolved stars.

There is some evidence for spherical $\text{Mg}_x\text{Fe}_{(1-x)}$ ($x = 0.1$) grains in dust shells around evolved stars (Molster & Waters 2003). Compositionally, these grains are magnesiowüstite found in meteorites (Rubin 1997; Brearley & Jones 1998) and IDPs (Rietmeijer 1998, 2002). The results suggest that DME condensates with calciowüstite compositions are present around young and evolved stars and they should be considered as a candidate compound in astronomical dust searches and among presolar grains in meteorites. The laboratory analyses of comet 81P/Wild 2 are capable of detecting a calciowüstite-like compound with up to ~ 28 -wt per cent CaO. Its presence in this comet would be support for these laboratory vapour phase condensation experiments that not only confirm some of the astronomical observations but also predict the presence of solids with particular compositions for dedicated astronomical searches. These solids formed at disequilibrium conditions but their metastable and their highly disordered amorphous nature offer the conditions to a varied and complex series of minerals evolving in natural extraterrestrial environments.

ACKNOWLEDGMENTS

We are grateful for a constructive review. FJMR and AP acknowledge the support from NASA grants NNG04GM48A and NNX07AI39G. JAN is grateful for support from the Cosmochemistry Program at NASA Headquarters. Samples were produced in the Astrochemistry Laboratory of the NASA Goddard Space Flight Center. The HRTEM analyses were performed in the Electron Microbeam Analyses Facility of the Department of Earth and Planetary Sciences at UNM.

REFERENCES

Allen W. C., Snow R. B., 1955, *J. Am. Ceram. Soc.*, 38, 264
 Bouwman J., Meeus G., de Koter A., Hony S., Dominik C., Waters L. B. F. M., 2001, *A&A*, 375, 950
 Baronnet A., 1984, *Fortschr. Mineral.*, 62, 187
 Bradley J. P., Brownlee D. E., 1986, *Sci*, 231, 1542
 Brearley A. J., Jones R. H., 1998, in Papike J. J., ed., *Reviews in Mineralogy*, Vol. 36. Mineral. Soc. America, Chantilly, p. 3
 De B. R., 1979, *Astrophys. Space Sci.*, 65, 191

Donn B., 1979, *Ap&SS*, 65, 167
 Duley W. W., Millar T. J., Williams D. A., 1979, *Ap&SS*, 65, 69
 Eitel W., 1965, *Silicate Science II, Dry Silicate Systems*. Academic Press Inc., New York
 Hadamcik E., Renard J.-B., Rietmeijer F. J. M., Levasseur-Regourd A. C., Hill H. G. M., Karner J. M., Nuth J. A., 2007, *Icarus*, 190, 660
 Hallenbeck S. L., Nuth J. A., III, Daukantes P. L., 1998, *Icarus*, 131, 198
 Hallenbeck S. L., Nuth J. A., III, Nelson R. A., 2000, *ApJ*, 535, 247
 Martin E., Vogel R., 1934, *Arch. Eisenhüttenwes.*, 8, 249
 Molster F. J., Bradley J. P., 2001, *Meteorit. Planet. Sci.*, 36, A140
 Molster F. J., Waters L. B. F. M., 2003, in Henning Th., ed., *Astromineralogy Lecture Notes in Physics*, Vol. 609. Springer, Heidelberg, p. 121
 Nelson R., Thiemens M., Nuth J., Donn B., 1989, in Ryder G, Sharpton V. L., eds, *Proc. 19th Lunar Planet. Sci. Conf.*, Cambridge Univ. Press and the Lunar and Planetary Institute, Cambridge, p. 559
 Newman A. C. D., 1987, *Chemistry of Clays and Clay Minerals*. Mineral. Soc. Monograph, Vol. 6. Longman Scientific and Technical, England
 Nuth J. A., Donn B., 1983, *J. Geophys. Res.*, 88, A847
 Nuth J. A., Donn B., 1984, *J. Geophys. Res.*, 89, B657
 Nuth J. A., III, Hallenbeck S. L., Rietmeijer F. J. M., 2000a, *JGR*, 105, 10387
 Nuth J. A., Rietmeijer F. J. M., Hallenbeck S. L., Withey P. A., Ferguson F., 2000b, in Sitko M. L., Sprague A. L., Lynch D. K., eds, *ASP Conf. Ser. Vol. 196, Thermal emission Spectroscopy and Analysis of Dust, Disks and Regoliths*. Astron. Soc. Pac., San Francisco, p. 313
 Nuth J. A., III, Rietmeijer F. J. M., Hill H. G. M., 2002, *Meteorit. Planet. Sci.*, 37, 1579
 Rietmeijer F. J. M., 1998, in Papike J. J., ed., *Reviews in Mineralogy*, Vol. 36. Mineral. Soc. America, Chantilly, p. 2
 Rietmeijer F. J. M., 2002, *Chemie der Erde*, 62, 1
 Rietmeijer F. J. M., Karner J. M., 1999, *JCP*, 110, 4554
 Rietmeijer F. J. M., Nuth J. A., 1991, in Ryder G., Sharpton V. L., eds, *Proc. Lunar Planet. Sci. Conf. Vol. 21. Lunar and Planetary Institute*, Houston, TX, p. 591
 Rietmeijer F. J. M., Nuth J. A., III, 2000, *Trans. AGU, EOS*, 81, 409
 Rietmeijer F. J. M., Nuth J. A., Mackinnon I. D. R., 1986, *Icarus*, 65, 211
 Rietmeijer F. J. M., Nuth J. A., III, Karner J. M., 1999a, *ApJ*, 527, 395
 Rietmeijer F. J. M., Nuth J. A., III, Karner J. M., 1999b, *PCCP*, 1, 1511
 Rietmeijer F. J. M., Nuth J. A., III, Karner J. M., Hallenbeck S. L., 2002, *PCCP*, 4, 546
 Rietmeijer F. J. M., Nuth J. A., III, Nelson R. N., 2004, *Meteorit. Planet. Sci.*, 39, 723
 Rietmeijer F. J. M., Nuth J. A., III, Rochette P., Marfaing J., Pun A., Karner J. M., 2006, *Am. Mineral.*, 91, 1688
 Rietmeijer F. J. M., Pun A., Kimura Y., Nuth J. A., III, 2008a, *Icarus*, 195, 493
 Rietmeijer F. J. M., Pun A., Nuth J. A., III, 2008b, *CPL*, 458, 355
 Rubin A. E., 1997, *Meteorit. Planet. Sci.*, 32, 231
 Seward T. P., III, 1970, in Alper A. M., ed., *Phase Diagrams, Materials Science and Technology*, Vol. 1. Academic Press Inc., London and New York, p. 295
 Stephens J. R., Kothari B. K., 1978, *M&P*, 19, 139
 Volten H., Muñoz O., Hovenier J. W., Rietmeijer F. J. M., Nuth J. A., Waters L. B. F. M., van der Zande W. J., 2007, *A&A*, 470, 377
 Wooden D. H., Harker D. E., Brearley A. J., 2005, in Krot A. N., Scott E. R. D., Reipurth B., eds, *Conf. Ser. Vol. 341, Chondrites and the Protoplanetary Disk*. Astron. Soc. Pac., San Francisco, p. 774

This paper has been typeset from a $\text{\TeX}/\text{\LaTeX}$ file prepared by the author.